11th International Symposium on Turbulence and Shear Flow Phenomena (TSFP11)
Southampton, UK, July 30 to August 2, 2019

LOGARITHMIC BEHAVIOUR OF ATTACHED STRUCTURES IN TURBULENT BOUNDARY LAYER

Jinyul Hwang

Department of Mechanical Engineering
KAIST
Daejeon 34141, Korea
j.yhwang@kaist.ac.kr

Hyung Jin Sung

Department of Mechanical Engineering
KAIST
Daejeon 34141, Korea
hjsung@kaist.ac.kr

ABSTRACT

Wall turbulence is a ubiquitous phenomenon in nature and engineering applications, yet predicting such turbulence is difficult due to its complexity. High-Reynolds-number turbulence, which includes most practical flows, is particularly complicated because of its wide range of scales. Although the attached-eddy hypothesis postulated by Townsend can be used to predict turbulence intensities and serves as a unified theory for the asymptotic behaviours of turbulence, the presence of attached structures has not been confirmed. Here, we demonstrate the logarithmic region of the turbulence intensity by identifying wall-attached structures of streamwise velocity fluctuations through direct numerical simulation of a moderate-Reynolds-number boundary layer. The wall-attached structures are self-similar and composed of multiple uniform momentum zones. The population density of the structures scales inversely with their height, which is reminiscent of the hierarchy of attached eddies. These findings suggest that the identified structures are prime candidates for Townsend's attached eddy and serve as cornerstones for understanding the multiscale phenomena of high-Reynolds-number boundary layers.

INTRODUCTION

Understanding wall-bounded turbulent flows is a long-standing challenge because of their complex and chaotic nature. The presence of a wall not only induces the formation of a thin shear layer close to the wall known as the turbulent boundary layer (TBL), where most of the energy consumption occurs in modern vehicles and pipelines, but also separates the TBL into different layers composed of multiscale fluid motions. These multiscale phenomena can be characterized in terms of the friction Reynolds number ($Re_\tau = \delta u_\tau/\nu$), which is the ratio of the viscous length scale ν/u_τ (ν is the kinematic viscosity, and u_τ is the friction velocity) and the flow thickness δ. Although much progress has been achieved in characterizing the onset of turbulence (Hof *et al.* 2004; Avila *et al.* 2011) and fully turbulent flows at low Re_τ (Kawahara *et al.* 2012), little progress has been made in the case of high Re_τ turbulence (Smits *et al.* 2011; Jiménez 2012; Barkley *et al.* 2015), which arises in engineering devices and atmospheric winds ($Re_\tau = O(10^{4-6})$), due to the wide range of scales that govern the transport of mass, momentum and heat.

To elucidate these multiscale phenomena, one approach is to examine the organized motions that retain their spatial coherence for relatively long periods, known as eddies or coherent structures, because these structures are responsible for the dynamical mechanisms and turbulence statistics (Robinson 1991; Adrian 2007; Jiménez 2018). The dominant coherent structures in the buffer layer are low-speed streaks and quasi-streamwise vortices (Kline *et al.* 1967) that are generated via a self-sustaining cycle (Hamilton *et al.* 1995). Above the buffer layer, the coherent structures are larger and more complex due to the presence of various scales. In this region, the mean streamwise velocity ($\overline{U}$) follows a logarithmic profile along y (Millikan 1938):

$$\overline{U}^+ = \kappa^{-1}\ln(y^+) + A, \tag{1}$$

where $\overline{U}^+ = \overline{U}/u_\tau$, $y^+ = u_\tau y/\nu$, κ is the von Kármán constant, A is the additive constant, and the overbar indicates an ensemble average. The logarithmic profile in Eq. (1) represents that the only relevant scales in this region are the wall-normal distance (y) and u_τ. At high Reynolds numbers, most of the bulk production and velocity drop originate from the logarithmic layer (Smits *et al.* 2011; Jiménez 2012). Townsend (1976) deduced a model for energy-containing eddies in the logarithmic layer whose size scales with y; these structures are 'attached' to the wall and self-similar. By assuming that the logarithmic layer consists of the superposition of the attached eddies and that the variation of the Reynolds shear stress across the layer is small compared to the viscous stress, the streamwise turbulence intensity is expressed as

$$\overline{u^2}^+ = B_1 - A_1\ln(y/\delta), \tag{2}$$

where A_1 and B_1 are constant. Perry & Chong (1982) extended this hypothesis by introducing hierarchies of geometrically similar eddies with the probability distribution function (PDF) that is inversely proportional to their height. Additionally, they predicted the emergence of a k_x^{-1} (k_x is the streamwise wavenumber) region in the spectrum that is the spectral signature of the attached eddies. In this regard, the attached-eddy hypothesis is a unified theory that links the asymptotic behaviors of the turbulence statistics of high-Reynolds-number flows.

Subsequently, several studies (Perry *et al.* 1986; Perry & Marusic 1995; Marusic 2001) have refined the model of Perry & Chong (1982) to test Townsend's hypothesis, but the Reynolds numbers are not sufficiently high enough to establish the logarithmic region. Recently, advanced measurements confirmed the presence of the k_x^{-1} region (Nickels *et al.* 2005) and the coexistence of logarithmic regions for $\overline{U}$ and $\overline{u^2}$ at $Re_\tau = O(10^{4\text{-}5})$ (Hultmark *et al.* 2012; Marusic *et al.* 2013). However, the central question that has not been resolved is as follows: what is the actual structure in the fully turbulent flow that accords with an attached eddy and forms the logarithmic region? Although Townsend (1976) and Perry & Chong (1982) proposed a particular shape of eddies based on the flow visualization results, these structures are modeled to formulate the inverse-power-law PDF and the constant shear stress.

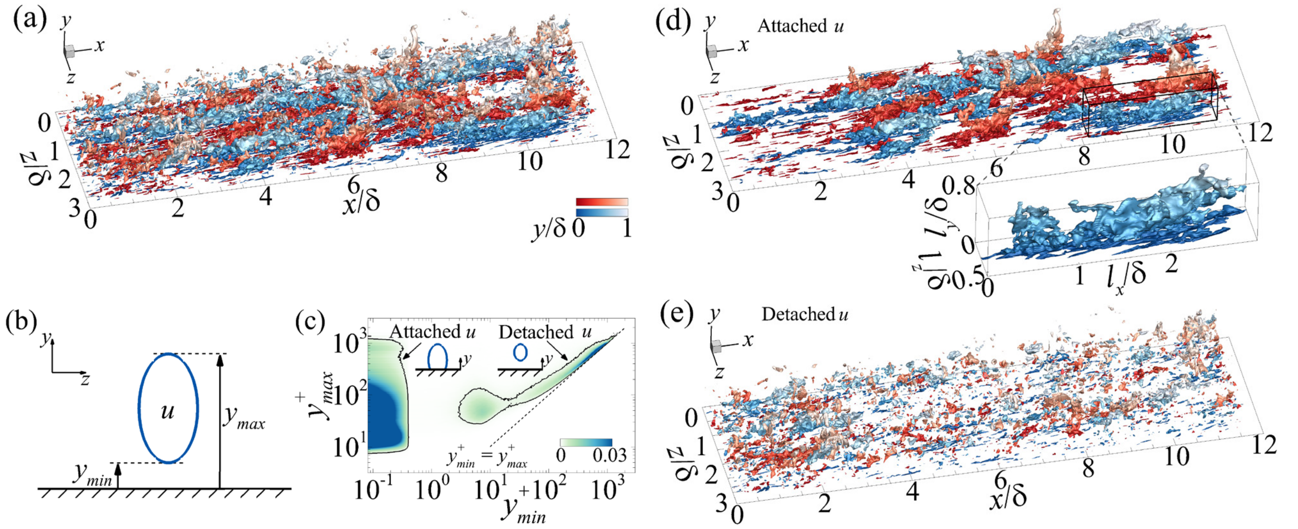

Figure 1. Clusters of streamwise velocity fluctuations (u) in turbulent boundary layer at Re_τ = 980. (a) Isosurfaces of positive- (red) and negative-u clusters (blue), $u(\boldsymbol{x}) = \pm 1.5u_{rms}(y,\ \delta_i)$, in the instantaneous flow field; δ_i is the height of the instantaneous turbulent/non-turbulent interface (TNTI). The brightness of the color indicates the wall distance. Here, the clusters, which cross the edges of the streamwise and spanwise domains, are excluded to represent the size of each cluster completely. (b) Schematic illustration of a u cluster in the cross-stream plane. The minimum (y_{min}) and maximum (y_{max}) wall distances of the individual cluster are shown. (c) The number of u clusters per unit wall-parallel area as a function of y_{min} and y_{max}. (d) Isosurfaces of wall-attached structures extracted from (a). The inset shows a magnified view of an attached negative-u structure that enclosed by the black box in the full domain. (e) Isosurfaces of detached structures extracted from (a).

Additionally, the k_x^{-1} region does not necessarily indicate the attached structure, because one coherent motion can carry the energy with a broad range of wavenumbers (Nickels & Marusic 2001) and the wavenumber at a given y does not reflect whether that motion is attached to the wall or is part of a detached one (Jiménez 2013).

To overcome these limitations, clusters of vortices (del Álamo & Jiménez 2006) and three-dimensional sweeps/ejections (Lozano-Durán *et al.* 2012) were identified in direct numerical simulation (DNS) of channel flows. These structures can be classified as either wall-attached or wall-detached. The former are self-similar and statistically dominant structures in the logarithmic layer. Hwang (2015) showed the self-similar motions with respect to y in a large-eddy simulation, which restricts the spanwise length scale of motions. Using a proper orthogonal decomposition, Hellström *et al.* (2016) found that the azimuthal length scales of the energetic modes are proportional to the distance from the wall. In addition, Baars *et al.* (2017) reported the self-similar region in the linear coherence spectrum where the coherence magnitude is quantified in a single streamwise/wall-normal aspect ratio. Although these identified coherent motions are reminiscent of Townsend's attached eddy in a sense of self-similarity, it has not been shown how these structures contribute to the logarithmic behavior of $\overline{u^2}$.

Here, we show the logarithmic region of $\overline{u^2}$ by identifying the wall-attached clusters of streamwise velocity fluctuations (u) from DNS data of zero-pressure-gradient TBL at $Re_\tau \approx 1000$. We focus on u clusters because long negative-u regions are associated with the net Reynolds shear force (Hwang *et al.* 2016a), and because the outer negative-u structures extend to the wall and interact with the near-wall streaks during the merging of the outer structures (Hwang *et al.* 2016b). We find that a group of u clusters over a wide range of scales is attached to the wall and self-similar. With these attached clusters, we can reconstruct the streamwise turbulent intensity from the superposition of the identified structures.

NUMERICAL DETAILS

The DNS data of the TBL (Hwang & Sung 2017; Yoon *et al.* 2018) are used in the present study. The DNS was performed using the fractional step method of Kim *et al.* (2002) to solve the Navier–Stokes equations and the continuity equation for the incompressible flow:

$$\frac{\partial U_i}{\partial t} + \frac{\partial}{\partial x_j} U_i U_j = -\frac{\partial P}{\partial x_i} + \frac{1}{\mathrm{Re}_{\delta_0}} \frac{\partial}{\partial x_j} \frac{\partial u_i}{\partial x_j}, \tag{3}$$

$$\frac{\partial U_i}{\partial x_i} = 0. \tag{4}$$

Here, all terms are normalized by the inlet boundary layer thickness δ_0 and the free-stream velocity U_∞. The inlet Reynolds number is defined as $\mathrm{Re}_{\delta_0} = U_\infty \delta_0 / \nu$. The no-slip boundary condition is applied at the wall, and the top boundary condition is $U = U_\infty, \partial V / \partial y = 0,$ and $W = 0$. In the spanwise direction, periodic boundary conditions are imposed. The convective boundary condition is applied at the exit. The inflow condition is set as a superposition of the Blasius velocity profile and the isotropic free-stream turbulence. The free-stream turbulence is generated by the Orr-Sommerfeld and Squire modes in the wall-normal direction and Fourier modes in time and in the spanwise direction (Jacobs & Durbin 2001). The computational domain is $2{,}300\delta_0 \times 100\delta_0 \times 100\delta_0$ in the streamwise (x), wall-normal (y) and spanwise (z) directions,

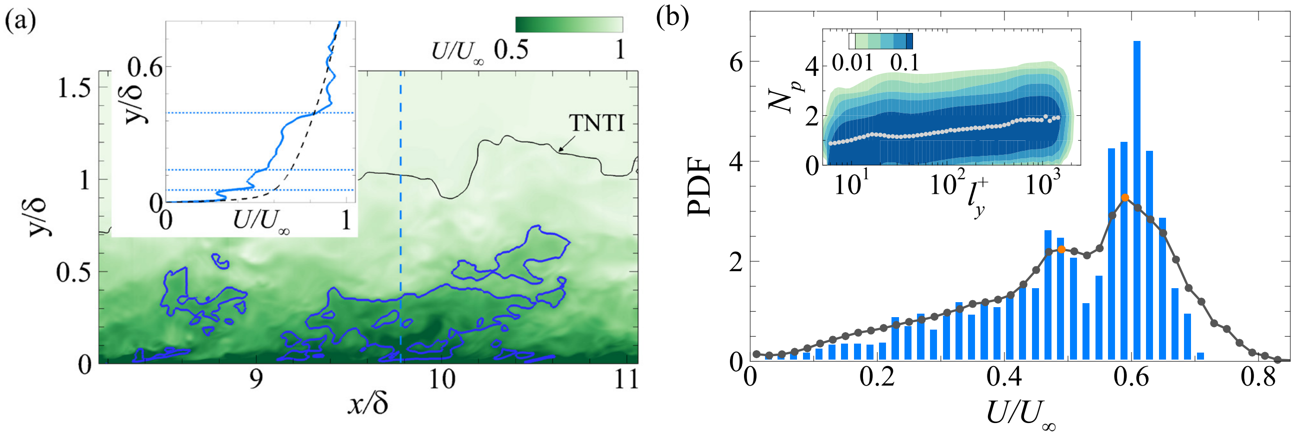

Figure 2. Uniform momentum zones in the attached structures of u. (a) Contour of the instantaneous streamwise velocity (U) in the x–y plane at $z/\delta = 0.26$; U_∞ is the free-stream velocity. The blue line is a slice of the object identified in figure 1(d). The black line indicates the TNTI. The inset shows a comparison of the instantaneous (solid line) and mean (dashed line) streamwise velocity profiles at $x/\delta = 9.8$ (indicated by the vertical dashed line in the contour). The horizontal dotted lines indicate step-like jumps of instantaneous velocity across the structure, which separate the zones of roughly constant U, known as uniform momentum zone (UMZ) [29]. (b) Histogram of U in the cross-stream plane of the identified object at $x/\delta = 9.8$, which contains the two distinct local maxima (at $U/U_\infty \approx 0.5$ and 0.6) that are associated with possible UMZs. The grey line shows the probability density function (PDF) of U within the identified object and the orange circles indicate the local maxima. The inset shows the joint PDF of the height (l_y) and the number of UMZs (n_p). The inserted dots indicate the mean n_p with respect to l_y. The contour levels are logarithmically distributed. Here, the superscript + denotes scaling with the viscous scale.

respectively. Given that the intermittent region appears at the turbulent/non-turbulent interface (TNTI), we define u ($= U - \overline{U}(y, \delta_i)$) by considering the height of the local TNTI (δ_i) to minimize the contamination of the fluctuations at the TNTI (Kwon *et al.* 2016). This decomposition can precisely detect the tall structures that span δ. The clusters of positive and negative u are the groups of connected points satisfying $|u(\boldsymbol{x})| > \alpha u_{rms}(y, \delta_i)$, where u_{rms} is the root mean square of u and α is the threshold. To characterize the irregular shapes of the u clusters (figure 1a), the connectivity of u was defined based on the six orthogonal neighbors of each node in Cartesian coordinates (del Álamo & Jiménez 2006; Lozano-Durán *et al.* 2012). Using the connectivity rule, the contiguous points are determined at a given node. As a result, we could determine the sizes of each cluster and the velocity information over a bounded volume of each object without making an a priori assumption or applying a filter. The threshold $\alpha = 1.5$ was chosen based on a percolation transition of the clusters; the results remained qualitatively unchanged within the transition; see Appendix in Hwang & Sung (2018) and Hwang & Sung (2019).

RESULTS AND DISCUSSION

The population density of clusters according to their minimum and maximum y (y_{min} and y_{max}) shows two distinct regions (figure 1c), yielding that the clusters are classified into two groups; wall-attached structures with $y_{min} \approx 0$ (figure 1d) and detached structures with $y_{min} > 0$ (figure 1e). The height of the attached structures ($l_y = y_{max} - y_{min} \approx y_{max}$) varies from the near-wall region to δ and they contribute 64% of the total volume of the clusters. In addition, each individual attached structure is composed of multiple uniform momentum zones (UMZs) in which U is roughly constant (Meinhart & Adrian 1995). As illustrated in figure 2(a), the sample attached structure extends from the wall to $y \approx 0.8\delta$ and in particular, the profile of U at $x/\delta = 9.8$ (inset in figure 2a) shows several jumps in velocity across the structure (indicated by dotted horizontal lines), separating zones of roughly uniform U. The UMZs produce local maxima in the histogram of U (Adrian et al. 2000). Figure 2(b) shows the histogram of U in the cross-stream plane of the identified structures at $x/\delta = 9.8$. Although there are several local maxima, the two at $U/U_\infty \approx 0.5$ and 0.6, which are the consequence of UMZs, are preserved when the data are accumulated over the entire structure (grey line). As shown in the inset of figure 2(b), the number of UMZs in each structure increases with increasing l_y, representing the hierarchical nature of attached structures (Perry & Chong 1982; de Silva *et al.* 2016). Moreover, these attached structures are geometrically self-similar. The distributions of their length (l_x) and width (l_z) with respect to l_y (figure 3a,b) show two distinct growth rates. For the buffer-layer structures ($l_y^+ < 60$), l_x and l_z increase gradually whereas those of the taller structures ($l_y^+ > 100$) grow rapidly until l_y is bounded by δ. For $l_y^+ > 100$, the mean l_x and l_z (circles) scale with l_y, representing a strong tendency for the self-similarity over a broad range, although there is some dispersion at a given l_y. Since the mean l_x and l_z indicate the sizes of representative structures, the dispersion would be associated with hierarchies at different stages of stretching (Perry & Chong 1982). Although the mean l_x is not linearly proportional to l_y, the inclination angle of the structures ranges from 8.8° to 16°; this trend is similar to the inclination angle of hairpin packets (Adrian *et al.* 2000). The mean l_z especially follows a linear law $l_z^+ \approx l_y^+$, indicating that the

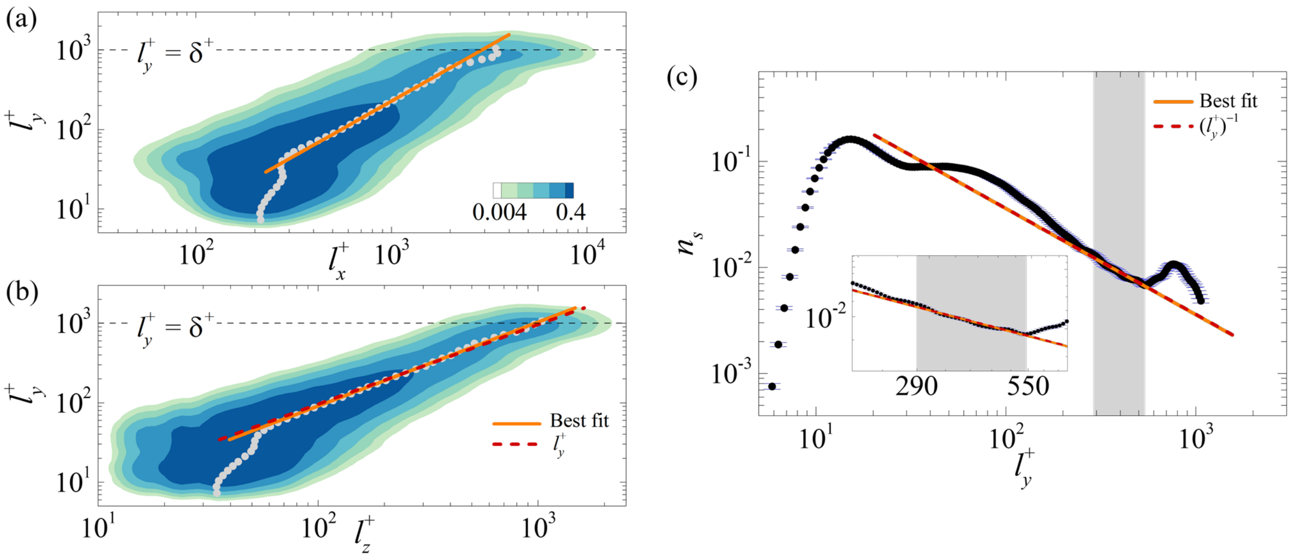

Figure 3. Self-similarity of attached structures and their population density. (a,b) Joint PDFs of the logarithms of the sizes (l_x and l_z) of the attached structures and of the height (l_y). The inserted dots indicate the mean l_x and l_z with respect to l_y. (a) The solid line is the best fit, $l_x^+ \sim (l_y^+)^{\gamma_1}$ with $\gamma_1 = 0.745$ of the data for $100 < l_y^+ < 550$. (b) The dashed line is $l_z^+ = 1.04 l_y^+$ and the solid line is the best fit, $l_z^+ \sim (l_y^+)^{\gamma_2}$ with $\gamma_2 = 0.949$ of the data for $l_y^+ > 100$. The contour levels are logarithmically distributed. (c) Population density of the attached clusters (n_s) with respect to their height l_y. The dashed line is $n_s \sim (l_y^+)^{-1}$ and the solid line is the best fit, $n_s \sim (l_y^+)^{\beta}$ with $\beta = -1.001$ of the data for $290 < l_y^+ < 550$. The inset shows a magnified view of the shaded region.

spanwise length scale of the structures is proportional to the distance from the wall.

The population density of the attached u structures versus l_y is examined to determine whether the attached structures are associated with the hierarchy length scales (Perry & Chong 1982; Perry *et al.* 1986). In figure 3(c), the distribution decays with l_y beyond the buffer layer, and in particular, it is inversely proportional to l_y for $290 < l_y^+ < 550$ (shaded region). Given the inverse-power-law PDF of hierarchy scales (Perry & Chong 1982) and the multiple UMZs in the attached structures of u (figure 2), the structures in the shaded region are hierarchies of self-similar eddies. Furthermore, a peak is evident at $l_y^+ \approx 800$, indicating the additional weighting for the large-scale structures. In other words, these large-scale structures are not geometrically self-similar in connection with the protrusions around $l_y^+ = \delta^+$ in figure 3(a,b). This behavior is consistent with the modified PDF of hierarchy scales (Perry *et al.* 1986), which was proposed to enable the more accurate prediction of the mean velocity defect and energy spectra.

The question then arises: does these attached structures actually form the logarithmic variation of $\overline{u^2}$? To answer this question, the streamwise turbulence intensity carried by attached structures with different heights $\overline{u_a^2(y,l_y)}$ is defined as

$$\overline{u_a^2(y,l_y)} = \left\langle \frac{1}{S_a(y,l_y)} \int_{S_a} u(\boldsymbol{x})u(\boldsymbol{x})dxdz \right\rangle, \qquad (5)$$

where S_a is the wall-parallel area of the structures with l_y at a given y and the angle brackets denote an ensemble anverage. In figure 4(a), the logarithmic region arises at $l_y^+ > 120$ and this region extends with increasing l_y. Although the magnitude of $\overline{u_a^2}$ is larger than that of $\overline{u^2}$ because the extracted structures are defined as $|u| > 1.5u_{rms}$, this result is remarkable considering the Reynolds number of the present TBL ($Re_\tau = 980$); the logarithmic behavior of $\overline{u^2}$ was observed at $Re_\tau = O(10^{4\text{-}5})$ in experiments (Hultmark *et al.* 2012; Marusic *et al.* 2013). Intriguingly, there is a logarithmic increase of the peak $\overline{u_a^2}$ with l_y^+ in $100 < l_y^+ < 550$ with a slope of 0.665 (see the inset in figure 4a). This result is in good agreement with the results for the slope of the increase in the peak $\overline{u^2}$ versus Re_τ obtained in a recent DNS 0.65 (Sillero *et al.* 2013) and in an experiments 0.63 (Marusic *et al.* 2017). Given the roots of attached structures, this agreement suggests that the identified structures are particularly important for predicting near-wall turbulence. In addition, the superposition of $\overline{u_a^2}$ ($\overline{u_{as}^2}$) over $290 < l_y^+ < 550$ is presented in figure 4(b). Here, $\overline{u_{as}^2}$ was computed by weighting the relative probability of the structures to the corresponding $\overline{u_a^2}$. To confirm the logarithmic variation of $\overline{u_{as}^2}$, the indicator function $y\partial \overline{u_{as}^2}^+ / \partial y$, which is constant in the logarithmic region, is also plotted. A plateau appears in $100 < y^+ < 0.18\delta^+$, verifying the presence of the logarithmic region formed by the attached structures.

CONCLUSIONS

We have demonstrated for the first time that the wall-attached structures of u are energy-containing motions satisfying the attached-eddy hypothesis, not only because they are self-similar to l_y, but also because there are three strong pieces of evidence: (i) the increase of the number of UMZs, identified within the wall-attached structures, with l_y, (ii) the

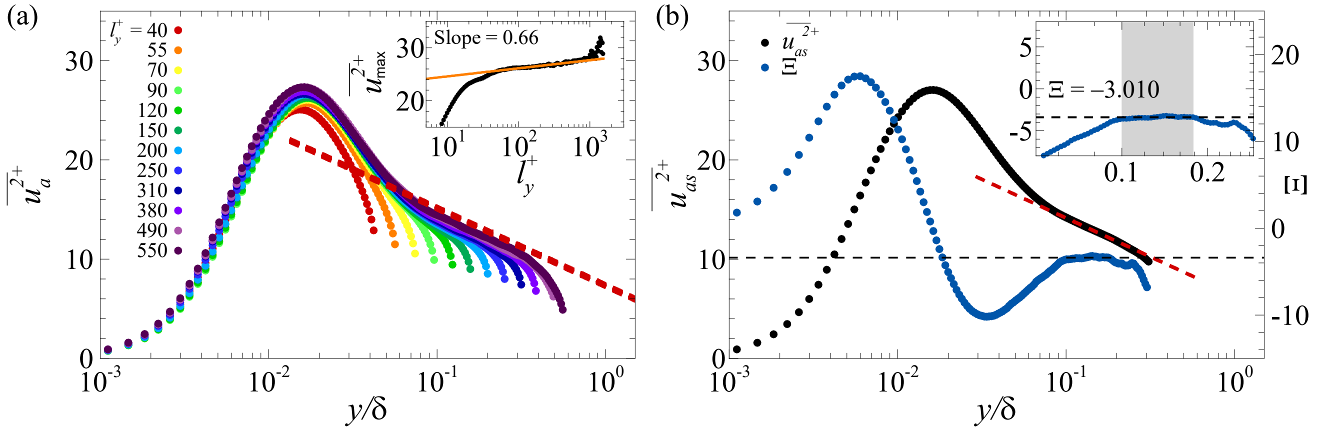

Figure. 4. Logarithmic behavior of the streamwise turbulence intensity carried by attached structures. (a) Wall-normal variations of the streamwise turbulence intensity ($\overline{u_a^2}$) within the attached structures of u for various l_y. The dashed line corresponding to the logarithmic variation is a guide for the eye. The inset shows the dependence of the peak magnitude of $\overline{u_a^2}$ on l_y. The solid line is the best fit, $\overline{u^2_{\max}}^+ = 0.66\ln(l_y^+) + 23.1$, of the data for $100 < l_y^+ < 550$. (b) Superposition of $\overline{u_a^2}$ carried by the attached structures with a population density that is inversely proportional to their height ($290 < l_y^+ < 550$ in figure 3b), $\overline{u_{as}^2}$. The blue dot indicates $\Xi = y\partial \overline{u_a^2}^+/\partial y$, which is the indicator function of the logarithmic law. The inset shows a magnified view of the region where there is a plateau ($\Xi = -3.010$) in the range $100 < y^+ < 0.18\delta^+$ (shaded region). The dashed line corresponds to $\overline{u_{as}^2}^+ = -3.010\ln(y/\delta) + 7.3$. Here, $\overline{u_{as}^2}$ and Ξ are plotted up to $y^+ = 290$.

inverse-power-law PDF, and (iii) the logarithmic variation of $\overline{u^2}$. Although we identified the attached structures in a TBL for a single Reynolds number, their hierarchical features will ensure their presence in high-Reynolds-number flows. We anticipate that examining the Reynolds-number effects on attached structures will improve the predictive model and exploring their dynamics will facilitate deeper insights into the multiscale energy cascade of wall turbulence.

ACKNOWLEDGEMENTS

This study was supported by a grant from the National Research Foundation of Korea (No. 2019M3C1B7025091), and partially supported by the Supercomputing Centre (KISTI).

REFERENCES

Adrian R. J. 2007 Hairpin vortex organization in wall turbulence. *Phys. Fluids* **19**, 041301.

Adrian R. J., Meinhart C. D. & Tomkins C. D. 2000 Vortex organization in the outer region of the turbulent boundary layer. *J. Fluid Mech.* **422**, pp. 1-54

Avila K., Moxey D., de Lozar A., Avila M., Barkley D. & Hof B. 2011 The onset of turbulence in pipe flow. *Science* **333**, pp. 192-196

Baars W. J., Hutchins N. & Marusic I. 2017 Self-similarity of wall-attached turbulence in boundary layers. *J. Fluid Mech.* **823**,

Barkley D., Song B., Mukund V., Lemoult G., Avila M. & Hof B. 2015 The rise of fully turbulent flow. *Nature* **526**, pp. 550

de Silva C. M., Hutchins N. & Marusic I. 2016 Uniform momentum zones in turbulent boundary layers. *J. Fluid Mech.* **786**, pp. 309-331

del Álamo J. C. & Jiménez J. 2006 Linear energy amplification in turbulent channels. *J. Fluid Mech.* **559**, pp. 205-213

Hamilton J. M., Kim J. & Waleffe F. 1995 Regeneration mechanisms of near-wall turbulence structures. *J. Fluid Mech.* **287**, pp. 317-348

Hellström L. H., Marusic I. & Smits A. J. 2016 Self-similarity of the large-scale motions in turbulent pipe flow. *J. Fluid Mech.* **792**,

Hof B., van Doorne C. W., Westerweel J., Nieuwstadt F. T., Faisst H., *et al.* 2004 Experimental observation of nonlinear traveling waves in turbulent pipe flow. *Science* **305**, pp. 1594-1598

Hultmark M., Vallikivi M., Bailey S. C. C. & Smits A. J. 2012 Turbulent pipe flow at extreme Reynolds numbers. *Phys. Rev. Lett.* **108**, pp. 094501

Hwang J., Lee J. & Sung H. J. 2016a Influence of large-scale accelerating motions on turbulent pipe and channel flows. *J. Fluid Mech.* **804**, pp. 420-441

Hwang J., Lee J., Sung H. J. & Zaki T. A. 2016b Inner–outer interactions of large-scale structures in turbulent channel flow. *J. Fluid Mech.* **790**, pp. 128-157

Hwang J. & Sung H. J. 2017 Influence of large-scale motions on the frictional drag in a turbulent boundary layer. *J. Fluid Mech.* **829**, pp. 751-779

Hwang J. & Sung H. J. 2018 Wall-attached structures of velocity fluctuations in a turbulent boundary layer. *J. Fluid Mech.* **856**, pp. 958-983

Hwang J. & Sung H. J. 2019 Wall-attached clusters for the logarithmic velocity law in turbulent pipe flow. *Phys. Fluids* pp. in press

Hwang Y. 2015 Statistical structure of self-sustaining attached eddies in turbulent channel flow. *J. Fluid Mech.* **767**, pp. 254-289

Jacobs R. & Durbin P. 2001 Simulations of bypass transition. *J. Fluid Mech.* **428**, pp. 185-212

Jiménez J. 2012 Cascades in wall-bounded turbulence. *Annual Review of Fluid Mechanics* **44**, pp. 27-45

Jiménez J. 2013 Near-wall turbulence. *Phys. Fluids* **25**, pp. 101302

Jiménez J. 2018 Coherent structures in wall-bounded turbulence. *J. Fluid Mech.* **842**, P1.

Kawahara G., Uhlmann M. & Van Veen L. 2012 The significance of simple invariant solutions in turbulent flows. *Annual Review of Fluid Mechanics* **44**, pp. 203-225

Kim K., Baek S. J. & Sung H. J. 2002 An implicit velocity decoupling procedure for the incompressible Navier-Stokes equations. *Int. J. Numer. Methods Fluids* **38**, pp. 125-138

Kline S. J., Reynolds W. C., Schraub F. & Runstadler P. 1967 The structure of turbulent boundary layers. *J. Fluid Mech.* **30**, pp. 741-773

Kwon Y., Hutchins N. & Monty J. 2016 On the use of the Reynolds decomposition in the intermittent region of turbulent boundary layers. *J. Fluid Mech.* **794**, pp. 5-16

Lozano-Durán A., Flores O. & Jiménez J. 2012 The three-dimensional structure of momentum transfer in turbulent channels. *J. Fluid Mech.* **694**, pp. 100-130

Marusic I. 2001 On the role of large-scale structures in wall turbulence. *Phys. Fluids* **13**, pp. 735-743

Marusic I., Baars W. J. & Hutchins N. J. P. R. F. 2017 Scaling of the streamwise turbulence intensity in the context of inner-outer interactions in wall turbulence. **2**, pp. 100502

Marusic I., Monty J. P., Hultmark M. & Smits A. J. 2013 On the logarithmic region in wall turbulence. *J. Fluid Mech.* **716**, R3.

Meinhart C. D. & Adrian R. 1995 On the existence of uniform momentum zones in a turbulent boundary layer. *Phys. Fluids* **7**, pp. 694-696

Millikan C. M. *Proceedings of the Fifth International Congress for Applied Mechanics, Harvard University and MIT, New York, 1938*. Wiley.

Nickels T. & Marusic I. 2001 On the different contributions of coherent structures to the spectra of a turbulent round jet and a turbulent boundary layer. *J. Fluid Mech.* **448**, pp. 367-385

Nickels T., Marusic I., Hafez S. & Chong M. 2005 Evidence of the k 1− 1 law in a high-Reynolds-number turbulent boundary layer. *Phys. Rev. Lett.* **95**, pp. 074501

Perry A. E. & Chong M. S. 1982 On the mechanism of wall turbulence. *J. Fluid Mech.* **119**, pp. 173-217

Perry A. E., Henbest S. & Chong M. S. 1986 A theoretical and experimental study of wall turbulence. *J. Fluid Mech.* **165**, pp. 163-199

Perry A. E. & Marusic I. 1995 A wall-wake model for the turbulence structure of boundary layers. Part 1. Extension of the attached eddy hypothesis. *J. Fluid Mech.* **298**, pp. 361-388

Robinson S. K. 1991 Coherent motions in the turbulent boundary layer. *Annual Review of Fluid Mechanics* **23**, pp. 601-639

Sillero J. A., Jiménez J. & Moser R. D. 2013 One-point statistics for turbulent wall-bounded flows at Reynolds numbers up to δ+≈ 2000. *Phys. Fluids* **25**, pp. 105102

Smits A. J., McKeon B. J. & Marusic I. 2011 High-Reynolds Number Wall Turbulence. *Annual Review of Fluid Mechanics* **43**, pp. 353-375

Townsend A. A. 1976. *The structure of turbulent shear flow*. Cambridge University Press.

Yoon M., Hwang J. & Sung H. J. 2018 Contribution of large-scale motions to the skin friction in a moderate adverse pressure gradient turbulent boundary layer. *J. Fluid Mech.* **848**, pp. 288-311